Front. Mater. Sci. 2025, 19(2): 250728
https://doi.org/10.1007/s11706-025-0728-x

RESEARCH ARTICLE

Continuous aramid fiber/unsaturated polyester resin composites with excellent interfacial and mechanical properties

Yan Zhang[1], Yinchun Hu (✉)[1], Kexin Chen[1], Zhibin Jin[1], Qi Lei[1], Yongcun Li[2], Chuanbo Cong[3], Qiong Zhou[3], and Yingying Wang (✉)[4]

1 College of Artificial Intelligence, Taiyuan University of Technology, Taiyuan 030024, China
2 National Demonstration Center for Experimental Mechanics Education, College of Aeronautics and Astronautics, Taiyuan University of Technology, Taiyuan 030024, China
3 College of New Energy and Materials, China University of Petroleum (Beijing), Beijing 102249, China
4 College of Safety and Ocean Engineering, China University of Petroleum (Beijing), Beijing 102249, China

ABSTRACT: The surface microstructure of continuous aramid fibers (AFs) is significant for AF/unsaturated polyester (UP) resin composites. The chemical modification of the AF surface is the key point to enhance mechanical properties of AF/UP composites. In this study, the polyethyleneimine (PEI)–polydopamine (PDA) coating was formed on the continuous AF surface via a one-step process. Morphologies and functional groups of PEI–PDA-coated AFs were studied. It was revealed that the interfacial bonding strength between PEI–PDA-AFs and the UP matrix was increased by 82.47% due to formation of the chemical bonding between amino groups on PEI and hydroxyl groups on UP. The tensile strength of the PEI–PDA-AF/UP composite reached 959.07 MPa, increased by 34.19% compared with that before modification. This study presents a simple and efficient method to prepare high-strength continuous AF/UP composites which could be used in engineering fields of deep-sea pipeline, aerospace, construction, military, safety, sports equipment, etc.

KEYWORDS: continuous aramid fiber; unsaturated polyester resin; polymer composite; interfacial shear strength; interlaminar shear strength

Contents

Received December 18, 2024; accepted April 6, 2025

E-mails: huyinchun@tyut.edu.cn (Y.H.), wyy@cup.edu.cn (Y.W.)

1 Introduction

High-performance fiber-reinforced polymers (FRPs) are composites formed by the combination of high-strength fibers with resin matrices. In this case, the resin matrix acts as a binder for the reinforcement, transferring the load between fibers [1], and fibers act as reinforcement for the resin matrix, providing the main support for the high strength of fiber composites. In comparison to short fibers, continuous long fibers have been demonstrated to be a more significant factor in improving the mechanical properties of fiber composites [2–3]. Consequently, FRPs are progressively supplanting traditional metallic structural materials due to their superior mechanical properties, favorable environmental stability, and light weight [4–8], which are extensively employed in aerospace, marine, automotive, military, biomedical, and rehabilitation aids sectors [9–14]. Aramid fibers (AFs) exhibit similar axial properties to inorganic fibers which have been studied widely [15–17]. Consequently, AFs have attracted considerable attention in the field of fiber-reinforced composites. Although AFs possess excellent properties, they are poorly bonded to the majority of resin matrices due to their high orientation and inert surface. The surface modification of AFs is the key to interface bonding between AFs and resin matrices.

In recent years, the surface modification of AFs has been performed mainly through chemical etching and grafting [18–23], plasma treatment [24–26], ultrasonic treatment [17,26], and γ-ray etching [27]. In contrast, chemical etching and grafting are employed to modify the surface of AFs via introducing reactive functional groups, such as amino and hydroxyl groups. Jia et al. adopted the grafting of 3-aminopropyltriethoxysilane (APS) on the AF surface, resulting in a significant improvement in the surface roughness, wettability, and surface free energy of AFs. Furthermore, the interfacial shear strength (IFSS) of resulting AF composites was increased by 51.03% from 36.33 to 54.87 MPa. Additionally, the modification process had no negative impact on the tensile strength of AFs, which making it a relatively environment-friendly approach [28]. Through the coordination of benzimidazole unit in the fiber structure with Fe^{3+}, Cheng et al. modified poly-*p*-phenylene-benzimidazole-terephthalamide (PBIA) followed by the grafting of polyethylene imine (PEI), and the resulting fibers exhibited an increase by 47% of the IFSS value [29]. The surface modification of fibers with polydopamine (PDA) and PEI has also been a hot topic in recent years. Zhu et al. developed double coatings of PDA and graphene oxide (GO) on AFs, leading to a 54% rise in the surface free energy while maintaining 93.4% of the tensile strength of AFs after ultraviolet (UV) irradiation for 168 h [30]. Zeng et al. grafted both PDA and GO on the AF surface, which exhibited an increase in IFSS by 210% owing to the formation of the resulting GO–PDA coating [31]. Gong et al. modified the AF surface with PDA and amino GO, resulting in improved interfacial adhesion properties. It was revealed that the IFSS value of amino GO–PDA-AF/epoxy (EP) reached 35.21 MPa, increased by 34% compared with that before grafting amino GO [32]. Li et al. used a modification method, in which poly(L-3,4-dihydroxyphenylalanine) (L-PDOPA) was successfully coated on the surface of AFs, leading to the formation of AFs with controllable layers. Then, a hydroxyl functionalized silane coupling agent (KH550) was grafted on the surface of L-PDOPA-coated AFs. The results show that interfacial adhesion properties (e.g., IFSS and interlaminar shear strength (ILSS)) of modified fiber/EP composites were greatly improved [33]. Wu et al. treated AFs with air plasma and increased the interfacial bond strength with unsaturated polyester (UP) by 65.60% [34]. Ruan et al. proposed an effective modification strategy for improving interface property through employing non-thermal atmospheric plasma to introduce active functional groups onto aramid paper. The modified composite demonstrated a 26% increase in the tensile strength and a 20% enhancement in the breakdown strength at best [35]. Yang et al. grew dense molybdenum disulfide (MoS_2) nanosheets on the PDA-functionalized AF surface via a simple hydrothermal method to improve the wettability between the AF surface and the polyhexahydrotriazine (PHT) resin, thereby enhancing the AF/resin interfacial bonding [36]. Li et al. used sulfone-functionalized poly(*p*-phthaloyl-*p*-phenylenediamine) (SPPTA) as the precursor to prepare the nanocoating solution. By further grafting epichlorohydrin (ECH) and shellac (SLC), the functional coating solution was obtained. The ECH–SLC-AF/EP composite showed excellent interfacial bonding and mechanical properties. The IFSS reached 43.7 MPa with a significant enhancement by 21.4%, and the flexural strength and

tensile strength were increased to 283 and 831 MPa, respectively [37]. Xu et al. enhanced mechanical properties of EP composites by gradually depositing PDA, PEI, and aminoated carbon nanotubes (NH_2-CNTs) on the AF surface using PDA as the initial layer. The ILSS, bending strength, and tensile strength of NH_2-CNTs–PEI–PDA-AF/EP were increased by 75%, 44.5%, and 14.9%, respectively, compared with those of the unmodified AF/EP composite [38].

Numerous studies indicate that chemical etching and grafting on AF surfaces could markedly enhance the interface bonding properties and mechanical strength of AF composites while minimizing the damage to AF simultaneously. Concurrently, dopamine (DA) could form the PDA coating under mild conditions which avoid damaging mechanical properties of AFs, and the AF surface with relatively high roughness, polarity, and reactive site density is achieved. PEI contains a great number of amino groups which can react with DA through both Schiff base reaction and Michael addition reaction under alkaline conditions. Amino groups on PEI could further enhance the polarity of the AF surface which also act as reactive groups with the UP resin matrix. Here, the PEI–PDA coating on the continuous AF surface was formed via a one-step process. The surface of the PEI–PDA-modified AF (PEI–PDA-AF) composite exhibited roughness and dense coating because of the Michael addition reaction and the Schiff base reaction between PEI and PDA. The PEI–PDA-AF/UP composite with excellent interfacial and mechanical tensile properties was prepared via the one-step AF surface modification and optimizing curing process. The amino groups on PEI–PDA-AFs could react with hydroxyl groups of the UP matrix. The interfacial bond strength of the PEI–PDA-AF/UP composite reached 40.60 MPa which was 82.47% higher than that of the AF/UP composite. The tensile strength of the PEI–PDA-AF/UP composite reached 959.07 MPa, indicating that this resulting material could be applied in extreme engineering fields such as deep-sea pipelines, aerospace, military, security, and sports equipment.

2 Experimental

2.1 Materials

AF (average diameter 14 μm, 1500 D) was purchased from Tayho Advanced Materials Co., Ltd. (Yantai, China). Dopamine hydrochloride (99%), trimethylolaminomethane (Tris), ethyl acetate (EA), PEI, and deionized water were from Shanghai Aladdin Biochemical Technology Co., Ltd. UP resin, cobalt naphthenate accelerator, and methyl ethyl ketone peroxide (MEKP) initiator were from Guangdong Yitong Chemical Co., Ltd. (China).

2.2 Preparation of PDA-AFs and PEI–PDA-AFs

AFs (each bundle of fibers of 20 cm length) were soaked in EA for 24 h to remove impurities. AFs were cleaned with deionized water and dried at 60 °C for 12 h. PDA-modified AFs (PDA-AFs) were prepared through dipping in the DA solution which refer to the method of Xu et al. [38]. A one-step process was used to prepare PEI–PDA-AFs. AFs were dipped in a mixed solution (the mass ratio of PEI to DA was 1:1, pH = 8.5) at 37 °C for 24 h, and shaker was used to ensure PDA and PEI deposited on the AF surface and single orientation of continuous PEI–PDA-AF bundles.

2.3 Preparation of AF/UP resin composites

UP resin, MEKP, and cobalt naphthenate in the mass ratio of 100:1:2 were homogeneously mixed. Briefly, 10 g UP resin and 0.1 g potassium ethyl ketone peroxide were firstly mixed and stirred well. Then 0.2 g cobalt naphthenate was added in the mixed solution. After AFs, PDA-AFs, or PEI–PDA-AFs were impregnated in the mixed solution, the excess resin was scraped off. The impregnated fibers were subsequently placed in the dried mound with released agent, and the contact pressure of 10 MPa was applied at the initial time. Finally it was transferred into the oven for curing when the UP resin became in the gel state. The process condition for curing was selected to be at 60 °C for 12 h.

2.4 Instruments and characterization

Scanning electron microscopy (SEM) was performed to observe the surface morphology before and after the AF modification, the post-pull-off cross-sectional morphology of the AF/UP transverse fiber bundle composite, and the surface morphology of the section of stretched samples. Prior to observation, the samples were sprayed with gold and accelerated at a voltage of 10 kV.

Fourier transform infrared spectroscopy (FTIR) was carried out to analyze functional groups on the surface of

AFs before and after the modification. The scanning resolution was 4 cm^{-1}, the scanning frequency was 32 times, and the scanning range was 400–4000 cm^{-1}.

The interfacial strength of the AF/UP composite was evaluated via the transverse fiber bundle tension (TFBT) test, and the tensile strength of the transverse fiber bundle composite (TFBC) was characterized [9,39]. The tests were conducted in accordance with the American Society for Testing and Materials Standard (ASTM) D638-2010, using a universal mechanical testing machine for tensile testing at room temperature, with a tensile speed of 2 $mm \cdot min^{-1}$, and the tensile testing was carried out until the damage occurred at the interface of between fibers and the resin.

The tensile test of the AF/UP composite was carried out according to GB/T 1040-1992 using a universal mechanical testing machine at room temperature. The maximum range of the load cell was 5 kN, and the tensile speed selected according to this standard was 2 $mm \cdot min^{-1}$.

2.5 Statistical analysis

Experimental data in this study was obtained from three parallel samples, and the results are presented as mean ± standard deviation (SD). Statistical significance was evaluated using one-way analysis of variance (ANOVA), and p value less than 0.05 was considered to indicate a significant difference ($*p < 0.05$, $**p < 0.01$, $***p < 0.001$).

3 Results and discussion

3.1 Surface modification of AFs

The microstructure of the AF surface was observed to determine the effect of AF surface modification, as illustrated in Fig. 1. Smooth surface with some grooves along the fibers was observed on untreated AF, created during the spinning process. The PDA-AF surface was significantly rough with many raised structures which was PDA coating formed through the oxidative self-polymerization of DA. The surface of PEI–PDA-AFs exhibited abundant lamellated stacked layers, along with a large dense coating, which resulted from the Michael addition and Schiff base reactions between PEI and PDA. The amino groups on PEI–PDA-AFs react with hydroxyl groups in the UP matrix, forming chemical bonds, which was very important for enhancing the interfacial bonding strength and overall mechanical properties of the composites.

Surface functional groups and chemical structures of AFs in different modification stages were studied to further verify the successful loading of PEI and PDA on the AF surface. FTIR spectra of AFs, PDA-AFs, and PEI–PDA-AFs were presented in Fig. 2. The peak at 3300 cm^{-1} was attributed to the N−H stretching vibration, while that at 815 cm^{-1} resulted from the C−H bending vibration. For AFs, the peak at 1633 cm^{-1} corresponded to the C=O stretching vibration, and the peak at 1512 cm^{-1} was assigned to the C=C stretching vibration [40–41]. Furthermore, the C−N stretching vibration peak of AFs was observed at 1306 cm^{-1}, and the region of 1700–1200 cm^{-1} was identified as the characteristic peak of AFs. The peaks observed at 2921 and 2853 cm^{-1} were identified as resulting from the asymmetric stretching vibration and symmetric stretching vibration of submethylene in PDA. This evidence supports that PDA coating was successfully deposited on the AF surface. PEI–PDA-AFs revealed a notable increase in the N−H stretching vibration peak at 3292 cm^{-1} in comparison to PDA-AFs. Additionally, the C=O stretching vibration peaks appeared at 815 cm^{-1}. The C−H bending vibrational peaks at 1633 cm^{-1} and the slight enhancement of the C−N stretching vibrational peaks at 1306 cm^{-1} provided evidence of the Michael addition reaction between PDA and PEI on the AF surface. Such functional group changes agreed with the microstructures of PDA-AFs and PEI–PDA-AFs.

The AF surface modification process and reaction mechanism were shown in Fig. 3. The PDA coating was deposited on the AF surface through the van Der Waals forces, hydrogen bonding, and π–π coupling self-polymerization [42–43]. The Michael addition reaction and Schiff base reaction between PEI and PDA resulted in the successful grafting of PEI on the PDA coating [44–45]. This process increased the roughness and polarity of the AF surface [46], thereby enhancing the stability of bonding between AFs and the UP matrix. Concurrently, amino groups on the PEI surface could react chemically with hydroxyl groups of UP, forming chemical bonds between the enhancer and the substrate, which further improved mechanical properties of the AF/UP composite.

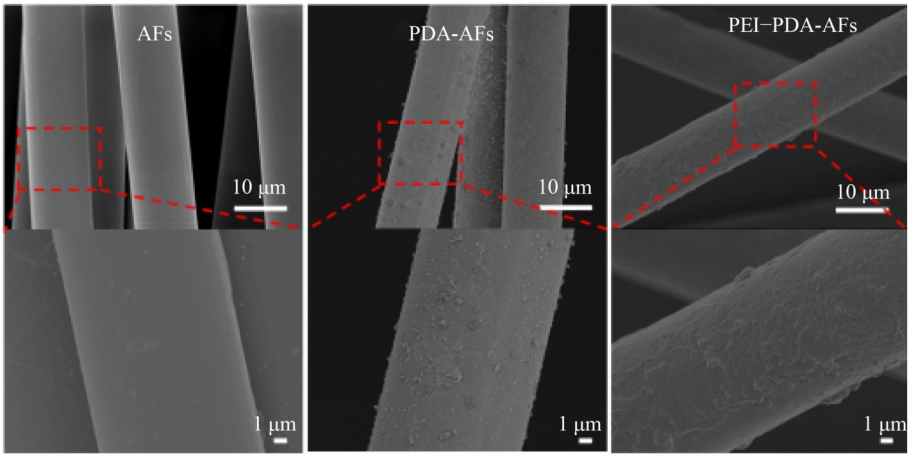

Fig. 1 SEM images of AFs, PDA-AFs, and PEI–PDA-AFs.

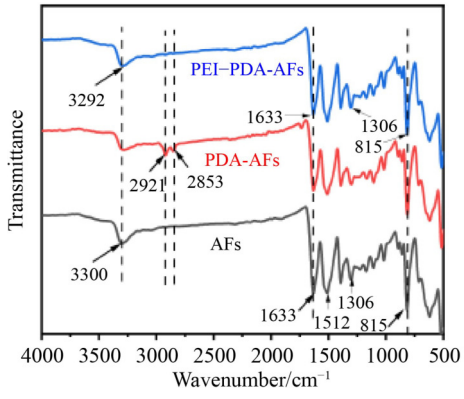

Fig. 2 FTIR spectra of AFs, PDA-AFs, and PEI–PDA-AFs.

3.2 Optimization of UP resins curing process

Matrix transfers stresses to reinforcing fibers during the stress damage and the UP matrix curing process is important for maintaining mechanical properties of the AF/UP composite. The UP curing process was optimized through testing mechanical properties of the UP matrix at different curing temperatures and durations. The stress–strain curves, tensile strength, Young's modulus, and elongation at break of the UP matrix under different curing processes were shown in Fig. 4. The tensile strength of UP ranged from 19.22 to 56.77 MPa, while the elongation at break ranged from 6.71% to 20.59% without brittle fracture. The lowest tensile strength and elongation at break (20.59%) were observed when UP was cured at 25 °C for 12 h, indicating that UP was not fully cured at this temperature. The tensile strength of UP increased gradually with the prolongation of the curing time at 60 °C, reaching 56.77 MPa after 24 h. The elongation at break tended to decrease with increasing the curing time, but the decrease was not significant. The tensile strength of UP increased significantly and the elongation at break substantially decreased when the curing temperature rose to 60 °C. Such results demonstrated that the curing temperature had a significant effect on the curing process of UP. Consequently, 60 °C was identified as the optimal curing temperature, and the tensile strengths of UP were 53.53 and 56.77 MPa when curing at 60 °C for 12 and 24 h, respectively. Considering the cost in the curing process, the process for curing the AF/UP composite was optimized at 60 °C for 12 h.

3.3 Interfacial properties of various AF/UP composites

TFBCs consisting of AF and UP were prepared for the tensile testing, and interfacial properties of AF and UP were characterized via the TFBT method. Figure 5 illustrated stress–strain curves and interfacial bond strengths of AF/UP, PDA-AF/UP, and PEI–PDA-AF/UP TFBCs. It is observed that the interfacial bond strength between AFs and the UP resin was only 22.25 MPa. After the deposition of PDA on AFs, the interfacial bond strength between PDA-AFs and UP increased to 29.12 MPa, indicating enhanced interface performance. Following the successful grafting of PEI–PDA on AFs, a notable alteration was observed in interfacial properties, with the interfacial bond strength between PEI–PDA-AFs and the UP resin reaching 40.60 MPa, which represented an increase by 82.47% compared to that of the AF/UP TFBC. Values of the elongation at break for AF/UP, PDA-AF/UP, and PEI–PDA-AF/UP TFBCs were 0.86%, 1.21%, and 1.75%, respectively, exhibiting an increasing

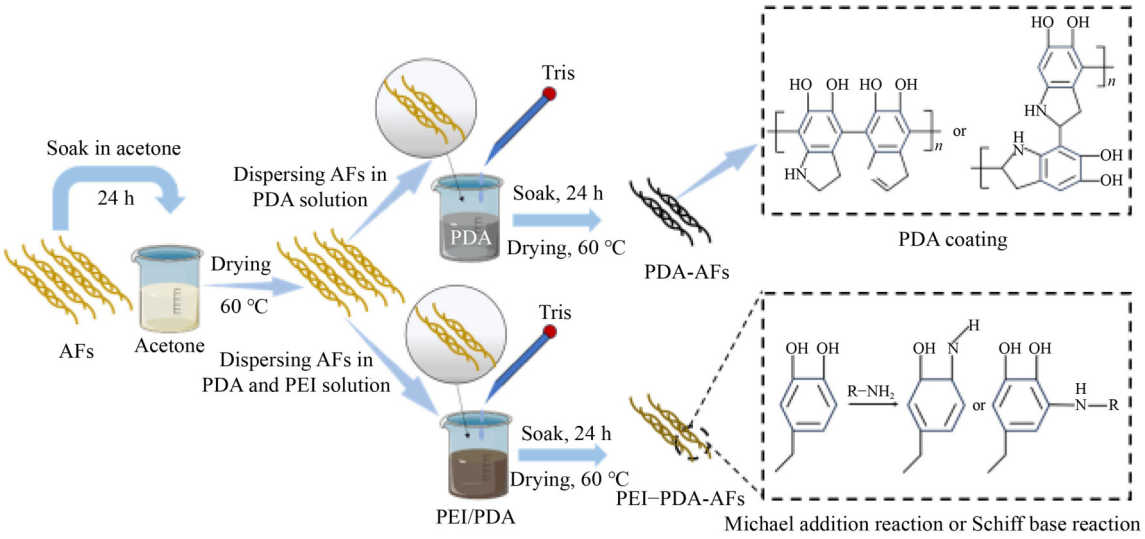

Fig. 3 AF surface modification process and reaction mechanism.

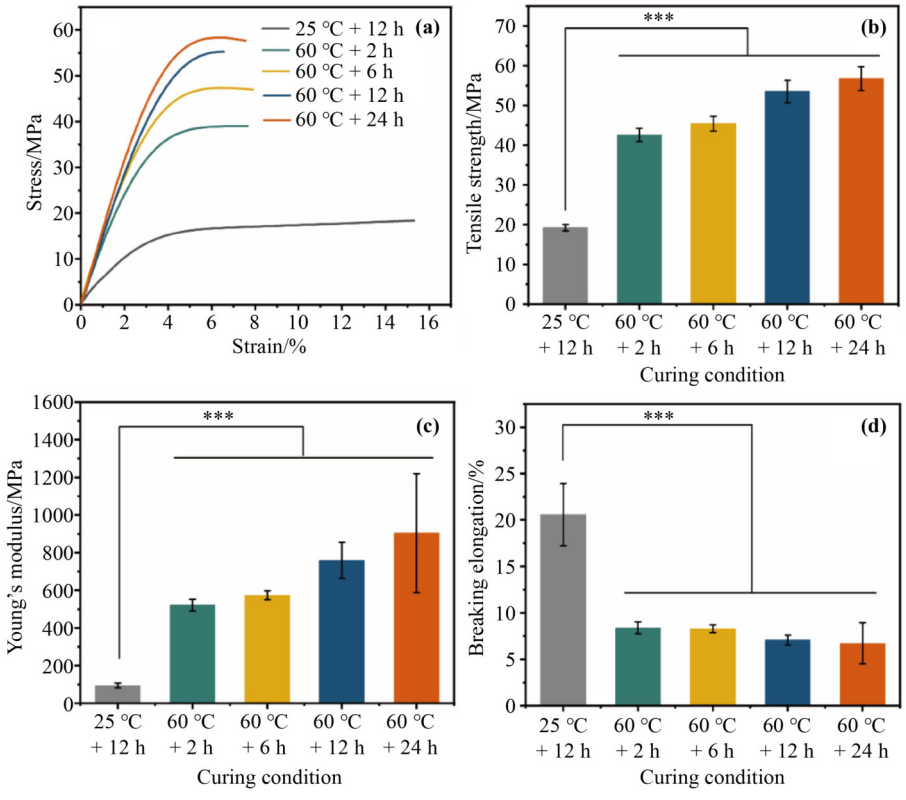

Fig. 4 (**a**) Stress–strain curves and values of (**b**) tensile strength, (**c**) Young's modulus, and (**d**) elongation at break of UP with different curing processes (***$p < 0.001$).

trend with the further reaction for compositional modification. The chemical combination between amino groups and hydroxyl groups results in a more robust interfacial bonding between PEI–PDA-AFs and UP, leading to enhanced values of the tensile strength and the elongation at break.

The cross-sectional morphologies of AF/UP, PDA-AF/UP, and PEI–PDA-AF/UP TFBCs after tensile fracture were shown in Fig. 6. The AF surface was notably smooth with little UP matrix attached, suggesting weak AF/UP interfacial bonding and low peeling energy between AFs and the UP matrix. After the successful coating of PDA

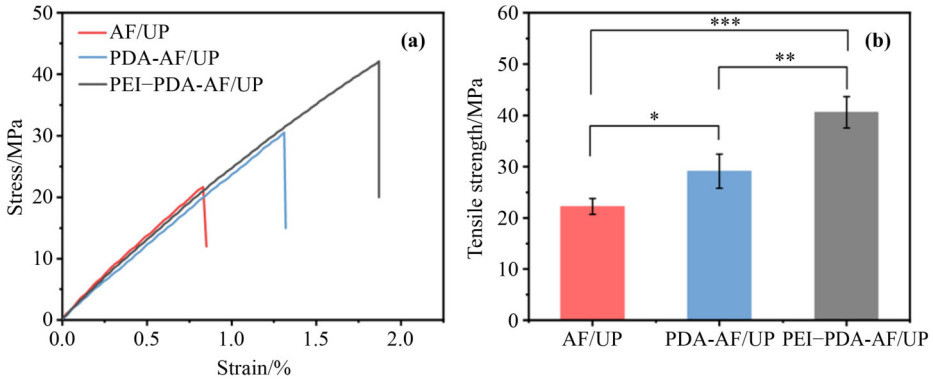

Fig. 5 (**a**) Tensile stress–strain curves and (**b**) interfacial bond strength values of AF/UP, PDA-AF/UP, and PEI–PDA-AF/UP TFBCs (*$p < 0.05$, **$p < 0.01$, ***$p < 0.001$).

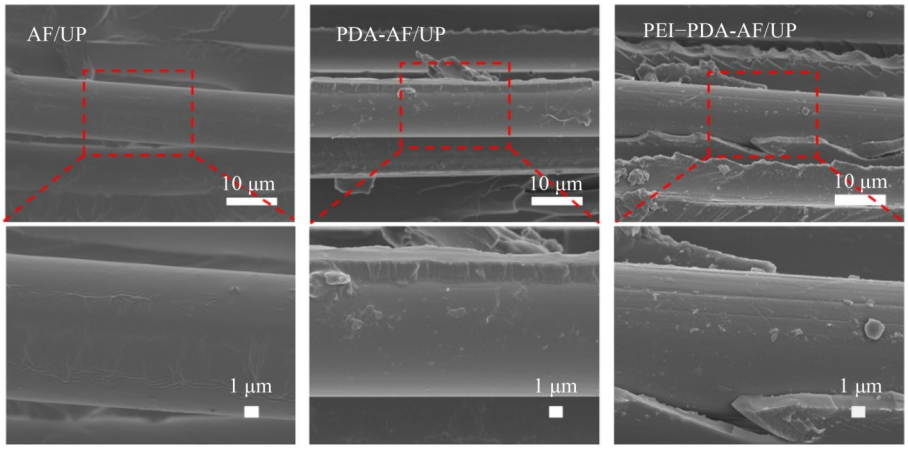

Fig. 6 Cross-sectional morphologies of AF/UP, PDA-AF/UP, and PEI–PDA-AF/UP TFBCs after tensile fracture.

on the AF surface, the residual UP matrix on the PDA-AF surface indicated that the PDA coating served as an adhesive linkage for the connection between PDA-AFs and UP during the peeling process, leading to a reduced likelihood of peeling off the UP matrix from PDA-AFs. The resin residue on the surface of PEI–PDA-AFs was more pronounced, and the UP matrix exhibited a multi-layer peeling phenomenon in the peeling damage on the PEI–PDA-AF surface. The bonding between PEI–PDA-AFs and the UP matrix was solid, diminishing the peeling damage to the PEI–PDA-AF/UP composite. The successful grafting of PEI strengthened the adhesion of the UP matrix to the surface of PEI–PDA-AFs, which reinforced interfacial properties of the AF/UP composite.

3.4 Mechanical properties of various AF/UP composites

The tensile strength serves as a crucial indicator of AF/UP composites. AF/UP composites with the AF mass content of 40% ± 2% were prepared in this study. Figure 7 shows stress–strain curves along with values of the tensile strength, the Young's modulus, and the elongation at break of UP and various AF/UP composites under the tensile loading. The tensile strength and Young's modulus of UP were 53.53 and 759 MPa, respectively. The tensile strength of the AF/UP composite reached 714.71 MPa, which was 13 times that of UP. The Young's modulus of the AF/UP composite reached 10.76 GPa, which was 14 times that of UP. AF/UP performs much better mechanical properties than UP because AF undertakes most of the tensile stress. The elongation at break of PEI–PDA-AF/UP showed no significant increase compared to that of AF/UP. The tensile strengths of PDA-AF/UP and PEI–PDA-AF/UP reached 836.85 and 959.07 MPa, which were increased by 17.09% and 34.19% in comparison with that of AF/UP, respectively. In this work, the tensile strength of PEI–PDA-AF/UP was significantly improved through optimizing the deposition

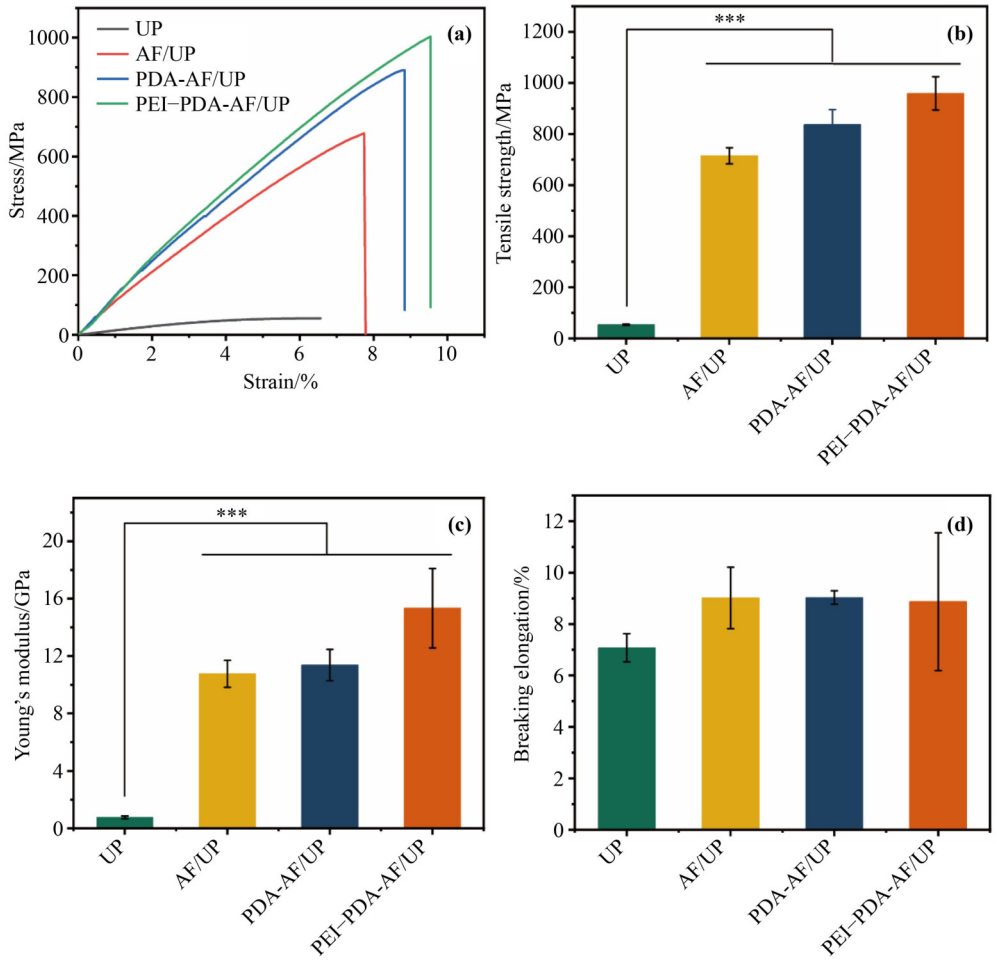

Fig. 7 (**a**) Tensile stress–strain curves and values of (**b**) tensile strength, (**c**) Young's modulus, and (**d**) elongation at break of UP, AF/UP, PDA-AF/UP, and PEI–PDA-AF/UP composites (***$p < 0.001$).

of PEI and PDA on the AF surface and the curing process of UP. By comparison, the tensile strength of NH_2-CNTs–PEI–PDA-AF/EP was only 477 MPa, which was 14.9% higher than that of R-AF/EP after the three-step deposition of NH_2-CNTs, PEI, and PDA reported by Xu et al. [38]. Table 1 summarizes effects of the AF surface modification on mechanical properties, such as TFBT, ILSS, IFSS, and tensile strength, of reported AF composites [33–38]. The fiber modification method in this study greatly enhanced TFBT by 82.47% and tensile strength by 34.19% compared to primary AF/UP which was superior to other methods. It is worth noting that the tensile strength of the AF/UP composite is related to the fiber content. In addition, specific experimental process details can also affect the mechanical properties of composites. Therefore, we should read Table 1 in conjunction with the experimental protocols in the original literature rather than simply comparing data.

Figure 8(a) shows macroscopic photographs and cross-sectional microstructures of AF/UP, PDA-AF/UP, and PEI–PDA-AF/UP composites after tensile fracture. Porous structures were observed after the pulling out of AFs, PDA-AFs, and PEI–PDA-AFs from the UP matrix, with composite structural failure caused by the fracture of AFs. AFs were the main load-bearing component for the AF/UP composite. AFs were neatly sectioned in tensile cross-section of the AF/UP composite due to the poor bonding strength of AFs and the UP matrix. It was difficult to pull PDA-AFs out of the UP matrix during the stretching process. The pulling out PDA-AF surface showed some rough-raised structures which was the PDA coating. The roughness of the PDA-AF surface enhanced the physical engagement between AFs and UP. PDA contains not only catechol groups but also amino groups on the side chain, which could react chemically with hydroxyl groups in UP. However, the number of amino

Table 1 Mechanical properties of AF composites in this work and in other reports

Modified AF composite	Matrix material	TFBT/MPa (η)	ILSS/MPa (η)	IFSS/MPa (η)	σ/MPa (η)	Ref.
5L-AF-R	EP	–	35/50.93 (45.50%)	14.80/22 (48.65%)	–	[33]
Air plasma-AF	EP	20.95/30.56 (45.87%)	–	–	–	[34]
90 s-plasma-AF	EP	–	–	–	38.13/47.99 (26%)	[35]
AF–MoS_2	PHT	–	–	35.80/62.90 (75.70%)	169.81/225 (32.50%)	[36]
AF–ECH–SLC	EP	–	–	36/43.70 (21.40%)	248/831 (235%)	[37]
NH_2-CNTs–PEI–PDA-AF	EP	–	46.8/81.90 (75.50%)	–	415/477 (14.90%)	[38]
PEI–PDA-AF	UP	22.25/40.60 (82.47%)	–	–	714.71/959.07 (34.19%)	This work

Notes: σ, tensile strength; η, enhancement percentage of the experimental group compared to the control group; AF, aramid fiber; CNT, carbon nanotube; ECH, epichlorohydrin; EP, epoxy; PDA, polydopamine; PEI, polyethylene imine; PHT, polyhexahydrotriazine; SLC: shellac; UP, unsaturated polyester.

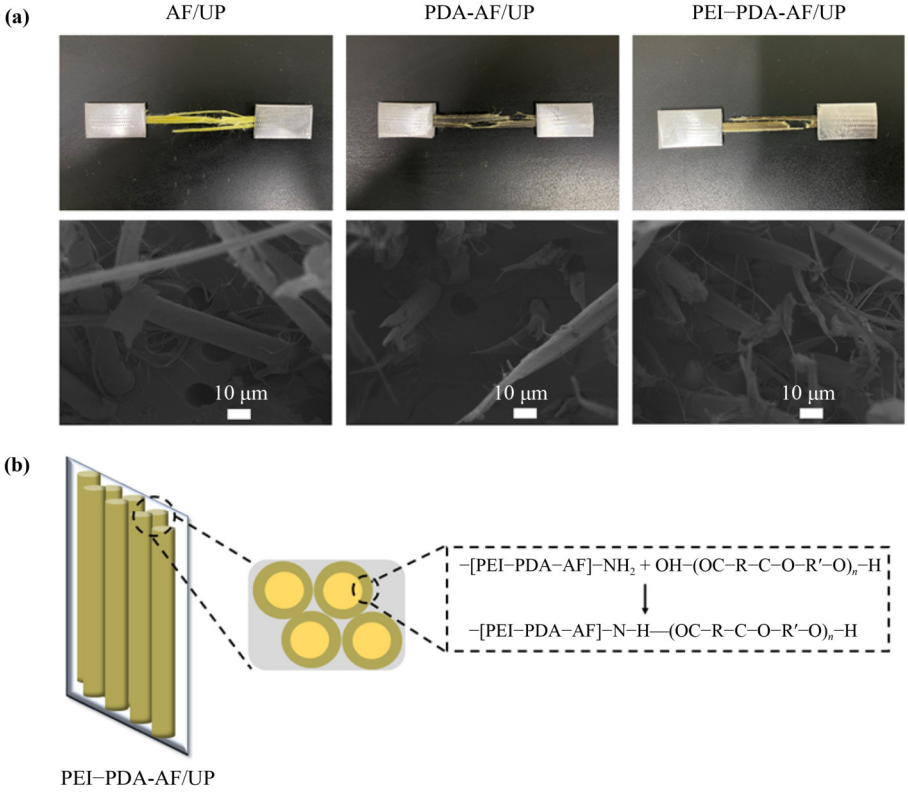

Fig. 8 (**a**) Macrophotographs and cross-sectional micromorphologies of AF/UP, PDA-AF/UP, and PEI–PDA-AF/UP composites after tensile fracture. (**b**) Bonding mechanisms of PEI–PDA-AFs and the UP matrix.

groups in PDA is small, so the chemical binding between PDA-AFs and UP is not significant. During the extraction process, PEI–PDA-AFs produced many filament structures along the axial direction of fibers. Amino groups on PEI had hydroxyl amination with hydroxyl group on the UP matrix (Fig. 8(b)). Between PEI–PDA-AFs and UP, there were not only mechanical bonding but also chemical bonding, making it more difficult for PEI–PDA-AFs to be pulled out from the UP matrix. As the primary reinforcement in the high-strength PEI–PDA-AF/UP composite, PEI–PDA-AFs played a key role in stress distribution and transfer during tensile deformation.

4 Conclusion

The high-strength continuous PEI–PDA-AF/UP composite was prepared through a one-step process of AF surface coating modification and optimizing curing process. The PEI–PDA-AF/UP composite exhibited the highest tensile strength of 959.07 MPa and the strongest interfacial bonding strength of 40.60 MPa. The interfacial

bonding strength and tensile strength of the PEI–PDA-AF/UP composite were enhanced by 82.47% and 34.19%, respectively, compared to those of the AF/UP composite. This improvement was attributed to the rough surface of PEI–PDA-AFs and the hydroxyl amination group bonding between the PEI–PDA-AF composite and the UP matrix. This study presents a simple and efficient modification approach for enhancing the mechanical properties of the continuous AF/UP composite. These findings provide critical guidance for designing and fabricating high-performance continuous AF/polymer composites.

Authors' contributions Yan Zhang: conceptualization, investigation, data curation, and writing - original draft; Yinchun Hu: investigation, project administration, supervision, and writing - review & editing; Kexin Chen: software, formal analysis, and validation; Zhibin Jin: investigation; Qi Lei: data curation; Yongcun Li: investigation; Chuanbo Cong: validation and investigation; Qiong Zhou: investigation; Yingying Wang: investigation and resources.

Declaration of competing interests The authors declare no potential conflicts of interest with respect to the research, authorship, and/or publication of this article.

Acknowledgements The authors gratefully acknowledge the financial support provided by National Key Research and Development Program of China: Key Materials Research of Non-metallic Flexible Risers for Deep Sea Mining (2022YFC2803702).

Data availability statement All data generated or analyzed during this study are included in this manuscript.

References

[1] Zhou A, Qin R Y, Chow C L, et al. Bond integrity of aramid, basalt and carbon fiber reinforced polymer bonded wood composites at elevated temperature. Composite Structures, 2020, 245: 112342

[2] Zhao Q, Liu C, Liang Y H, et al. Integration 3D printing of bionic continuous carbon fiber reinforced resin composite. Materials Research Express, 2021, 8(9): 095602

[3] Liang Y H, Liu C, Zhao Q, et al. Bionic design and 3D printing of continuous carbon fiber-reinforced polylactic acid composite with barbicel structure of eagle-owl feather. Materials, 2021, 14(13): 3618

[4] Fang C, Hu P, Dong S, et al. An efficient hydrothermal transformation approach for construction of controllable carbon coating on carbon fiber from renewable carbohydrate. Applied Surface Science, 2019, 491: 478−487

[5] Randall J D, Eyckens D J, Servinis L, et al. Designing carbon fiber composite interfaces using a 'graft-to' approach: surface grafting density versus interphase penetration. Carbon, 2019, 146: 88−96

[6] Yang C, Wu H, Dai Y, et al. Self-enhancement in aramid fiber by filling free hydrogen bonding interaction sites in macromolecular chains with its oligomer. Polymer, 2019, 180: 121687

[7] Dai Y, Han Y T, Yuan Y H, et al. Synthesis of heterocyclic aramid fiber based on solid-phase cross-linking of oligomers with reactive end group. Macromolecular Materials and Engineering, 2018, 303(8): 1800076

[8] Lv J W, Wang B, Ma Q, et al. Interfacially enhancement of PBO/epoxy composites by grafting MWCNTs onto PBO surface through melamine as molecular bridge. Materials Research Express, 2018, 5(6): 065006

[9] Qi G C, Zhang B M, Du S Y. Assessment of F-III and F-12 aramid fiber/epoxy interfacial adhesions based on fiber bundle specimens. Composites Part A: Applied Science and Manufacturing, 2018, 112: 549−557

[10] Wagih A, Sebaey T A, Yudhanto A, et al. Post-impact flexural behavior of carbon-aramid/epoxy hybrid composites. Composite Structures, 2020, 239: 112022

[11] Zhang B, Jia L H, Tian M, et al. Surface and interface modification of aramid fiber and its reinforcement for polymer composites: a review. European Polymer Journal, 2021, 147: 110352

[12] Mao L B, Gao H L, Yao H B, et al. Synthetic nacre by predesigned matrix-directed mineralization. Science, 2016, 354(6308): 107−110

[13] Gao H L, Chen S M, Mao L B, et al. Mass production of bulk artificial nacre with excellent mechanical properties. Nature Communications, 2017, 8(1): 287

[14] Zhang Y W, Zheng J L, Yue Y H, et al. Bioinspired LDH-based hierarchical structural hybrid materials with adjustable mechanical performance. Advanced Functional Materials, 2018, 28(49): 1801614

[15] Yue C Y, Padmanabhan K. Interfacial studies on surface modified Kevlar fibre/epoxy matrix composites. Composites Part B: Engineering, 1999, 30(2): 205−217

[16] Watanabe H, Furukawa M, Takata T, et al. Surface improvements of aramid fibers by physical treatments. Macromolecular Symposia, 2000, 159(1): 131−142

[17] Liu L, Huang Y D, Zhang Z Q, et al. Ultrasonic treatment of aramid fiber surface and its effect on the interface of aramid/epoxy composites. Applied Surface Science, 2008, 254(9): 2594−2599

[18] Day R J, Hewson K D, Lovell P A. Surface modification and its effect on the interfacial properties of model aramid-fiber/epoxy composites. Composites Science and Technology, 2002, 62(2): 153−166

[19] Liu T M, Zheng Y S, Hu J. Surface modification of aramid fibers with novel chemical approach. Polymer Bulletin, 2011, 66(2): 259−275

[20] Park S J, Seo M K, Ma T J, et al. Effect of chemical treatment of Kevlar fibers on mechanical interfacial properties of composites. Journal of Colloid and Interface Science, 2002, 252(1): 249−255

[21] Imielińska K, Guillaumat L. The effect of water immersion ageing on low-velocity impact behavior of woven aramid–glass fibre/epoxy composites. Composites Science and Technology, 2004, 64(13−14): 2271−2278

[22] Cheng Z, Zhang L J, Jiang C, et al. Aramid fiber with excellent interfacial properties suitable for resin composite in a wide polarity range. Chemical Engineering Journal, 2018, 347: 483−492

[23] Eyckens D J, Arnold C L, Randall J D, et al. Fiber with butterfly wings: creating colored carbon fibers with increased strength, adhesion, and reversible malleability. ACS Applied Materials & Interfaces, 2019, 11(44): 41617−41625

[24] Xi M, Li Y L, Shang S Y, et al. Surface modification of aramid fiber by air DBD plasma at atmospheric pressure with continuous on-line processing. Surface and Coatings Technology, 2008, 202(24): 6029−6033

[25] Jia C X, Chen P, Liu W, et al. Surface treatment of aramid fiber by air dielectric barrier discharge plasma at atmospheric pressure. Applied Surface Science, 2011, 257(9): 4165−4170

[26] Oldham T, Simon K, Ferriell D R, et al. Highly uniform activation of carbon fiber reinforced thermoplastics by low-temperature plasma. ACS Applied Polymer Materials, 2019, 1(10): 2638−2648

[27] Zhang Y H, Huang Y D, Liu L, et al. Effects of γ-ray radiation grafting on aramid fibers and its composites. Applied Surface Science, 2008, 254(10): 3153−3161

[28] Jia C Y, Zhang R Z, Yuan C C, et al. Surface modification of aramid fibers by amino functionalized silane grafting to improve interfacial property of aramid fibers reinforced composite. Polymer Composites, 2020, 41(5): 2046−2053

[29] Cheng Z, Chen C, Huang J Y, et al. Nondestructive grafting of PEI on aramid fiber surface through the coordination of Fe(III) to enhance composite interfacial properties. Applied Surface Science, 2017, 401: 323−332

[30] Zhu J J, Yuan L, Guan Q B, et al. A novel strategy of fabricating high performance UV-resistant aramid fibers with simultaneously improved surface activity, thermal and mechanical properties through building polydopamine and graphene oxide bi-layer coatings. Chemical Engineering Journal, 2017, 310(Part 1): 134−147

[31] Zeng L, Liu X Q, Chen X G, et al. Surface modification of aramid fibres with graphene oxide for interface improvement in composites. Applied Composite Materials, 2018, 25(4): 843−852

[32] Gong X Y, Liu Y Y, Wang Y S, et al. Amino graphene oxide/dopamine modified aramid fibers: preparation, epoxy nanocomposites and property analysis. Polymer, 2019, 168: 131−137

[33] Li Z M, Liu B H, Kong H J, et al. Layer-by-layer self-assembly strategy for surface modification of aramid fibers to enhance interfacial adhesion to epoxy resin. Polymers, 2018, 10(8): 820

[34] Wu Z C, Ma R T, Ai Z J, et al. *In situ* interfacial evaluation of aramid/epoxy composites by interfacial stress transfer characteristics. Review of Scientific Instruments, 2024, 95: 075110

[35] Ruan H O, Wang W H, Liu X, et al. Interface engineering via non-thermal atmospheric plasma for highly tensile insulating epoxy-impregnated aramid composite paper. Composites Science and Technology, 2024, 257: 110844

[36] Yang Y, Min C, Xu Z, et al. Strong interfacial modified aramid fabric reinforced degradable thermosetting composites: reinforcing and tribological effects. Materials Today: Chemistry, 2022, 24: 100795

[37] Li T, Wang Z X, Cao Y T, et al. Preparation of robust aramid/epoxy composites through enhancing the interface performance by nanocoating solution. Fibers and Polymers, 2022, 23(4): 1077−1088

[38] Xu T, Tian J, An L Z, et al. Study on the construction of dopamine/poly(ethyleneimine)/aminoated carbon nanotube multilayer films on aramid fiber surfaces to improve the mechanical properties of aramid fibers/epoxy composites. ACS Omega, 2022, 7(40): 35610−35625

[39] Qi G C, Zhang B M, Du S Y, et al. Estimation of aramid fiber/epoxy interfacial properties by fiber bundle tests and multiscale modeling considering the fiber skin/core structure. Composite Structures, 2017, 167: 1−10

[40] Chen Y, Yin Q, Zhang X M, et al. Rational design of multifunctional properties for styrene-butadiene rubber reinforced by modified Kevlar nanofibers. Composites Part B: Engineering, 2019, 166: 196−203

[41] Yang M, Cao K Q, Sui L, et al. Dispersions of aramid nanofibers: a new nanoscale building block. ACS Nano, 2011, 5(9): 6945−6954

[42] Wang Z X, Lau C H, Zhang N Q, et al. Mussel-inspired tailoring of membrane wettability for harsh water treatment. Journal of Materials Chemistry A: Materials for Energy and Sustainability, 2015, 3: 2650−2657

[43] Dreyer D R, Miller D J, Freeman B D, et al. Perspectives on poly(dopamine). Chemical Science, 2013, 4(10): 3796−3802

[44] Chen L, Du Y Z, Huang Y D, et al. Hierarchical poly(*p*-phenylene benzobisoxazole)/graphene oxide reinforcement with

multifunctional and biomimic middle layer. Composites Part A: Applied Science and Manufacturing, 2016, 88: 123−130

[45] Zhao W R, Zhang W, Liu Y, et al. Fe^{3+} ions induced rapid co-deposition of polydopamine–polyethyleneimine for monovalent selective cation exchange membrane fabrication. Separation and Purification Technology, 2022, 300: 121802

[46] Chen W, Yu Y Y, Liu W J, et al. Dual-functional amino-quinone coatings on cotton fabrics assembled with different molecular weight polyethyleneimine and dopamine. Progress in Organic Coatings, 2023, 174: 107306